Materials Science in Semiconductor Processing 90 (2019) 190–197

Contents lists available at ScienceDirect

Materials Science in Semiconductor Processing

journal homepage: www.elsevier.com/locate/mssp

Effect of CeO_2 content in morphology and optoelectronic properties of TiO_2-CeO_2 nanoparticles in visible light organic degradation

Julieth Carolina Cano-Franco, Mónica Álvarez-Láinez*

Design Engineering Research Group–GRID, Universidad Eafit, Carrera 47 sur #35-75 Medellín, Antioquia, Colombia

ARTICLE INFO

Keywords:
Semiconductor heterojunction
Nanoparticles
TiO_2
CeO_2
Band gap energy

ABSTRACT

TiO_2 is a semiconductor widely used in photocatalytic degradation of organic pollutants due to its band gap energy. However, its absorption range is restricted only to UV radiation that is less than 10% of solar light. With the aim of increasing the adsorption area on TiO_2 nanoparticles a modified sol-gel method was used to produce a smaller particle size, and to extend the absorption range to the visible spectrum, TiO_2 nanoparticles were synthesized with different CeO_2 contents to generate semiconductor heterojunction between them. The crystallographic, morphological, and optoelectronic characteristics of these TiO_2-CeO_2 nanoparticles were studied, and two crystalline phases were differentiated: anatase for TiO_2 and fluorite for CeO_2. An increase in the CeO_2 content produced crystallite sizes between 6.5 nm and 12.0 nm. TiO_2-CeO_2 nanoparticles showed morphological properties such as small particle size, heterogeneous surface and high BET surface area compared to bare commercial TiO_2. These features involve a positive effect of CeO_2 in TiO_2 nanoparticles surface, thus TiO_2-CeO_2 nanoparticles exhibit enhanced optoelectronic properties caused by a decrease in the effective band gap and red-shift in the electromagnetic spectrum. In addition, methylene blue degradation showed that TiO_2-CeO_2 nanoparticles are suitable for high photocatalytic activity application under visible light.

1. Introduction

Titanium dioxide (TiO_2) is one of the most studied photocatalytic materials because it efficiently converts solar energy into effective chemical energy and, as a consequence, it is used to degrade organic pollutants present in air and water, absorb heavy metals, and decompose bacteria and viruses, amongst others [1,2]. Although TiO_2 has a wide band gap of 3.2 eV, it can only absorb UV radiation (which represents only 3–5% of sunlight) [3]. TiO_2 also exhibits high rate pair hole-electron recombination, which is unfavorable for photocatalytic applications.

Several strategies such as metal semiconductor modification, doping with no-metal elements, and coupled semiconductors have been used to improve TiO_2 photocatalytic activity. Usually, this has been done to promote the separation of photogenerated charges in the surface, decrease electron-hole recombination and extend the radiation absorption range by a red-shift toward visible light [3]. For this, some semiconductors such as Bi_2S_3, CdS, ZrO_2 and CeO_2 have been combined with TiO_2 [4–6]. Apart from promote charge separation, the band gap narrowing by semiconductor heterojunction can produce an enhance in the reaction kinetics on the semiconductor surface and thus improve the efficiency in photocatalysis [7].

CeO_2 has unique properties such as high activity of redox couple Ce^{4+}–Ce^{3+}, noble metal reduction and oxidation reactions, oxygen, hydrogen and sulphur storage and release, and oxygen vacancies production [8]. CeO_2 is a catalytic material that absorbs mainly in the visible range, thus, CeO_2 coupled to TiO_2 has shown an upgrade to separate photogenerated charges, changing the light absorption range [9].

TiO_2-CeO_2 nanostructure has been manufactured by different methods: aerosol assisted chemical vapor deposition (AACVD) [10], co-precipitation [11], and sol-gel technique [12]. The last method is widely used because of its relative simplicity and versatility that allows the formation of a variety of metallic oxides by hydrolysis and condensation reactions of metal alkoxide precursors. Moreover, the final properties of nanoparticles can be modified to enhance certain characteristics. Several variables are involved in the sol-gel synthesis, such as metallic oxide precursor types, solvents, catalysts, and complex agents employed [17]. A critical point in TiO_2 sol-gel synthesis is the high reactivity of TiO_2 metallic alkoxides precursors, hence its stabilization is necessary by complexation reactions to avoid the fast condensation and precipitate formation [18].

Several authors have studied the chemical modification of titanium tetraisopropoxide (TTIP) with acetylacetone (Acac) [18–21], finding

* Corresponding author.
E-mail address: malvar26@eafit.edu.co (M. Álvarez-Láinez).

https://doi.org/10.1016/j.mssp.2018.10.017
Received 12 February 2018; Received in revised form 15 October 2018; Accepted 16 October 2018
Available online 31 October 2018
1369-8001/

that Acac reacts quickly with TTIP as a strong chelating ligand that reduces the reactivity of the metallic alkoxide. The modification of TTIP by Acac produces a new titanium complex precursor to yield stable gels, in sol-gel synthesis, and a smaller particle size. In addition, the secondary compounds from those reactions are easily removed solvents. Regarding the TiO_2-CeO_2 combined nanoparticles, some authors study sol-gel synthesis but they do not modify the reactivity of TiO_2 precursors. They add capping, stabilizing or dispersing agents to limit the growth and to prevent agglomeration of nanoparticles [22–24]. Thus, these agents must be removed completely in calcination processes. In our work, we propose the addition of Acac in the sol-gel synthesis of TiO_2-CeO_2 nanoparticles with the aim of reducing the reactivity of TTIP, forming stable gels and thus, producing small particles size.

Sol-gel TiO_2 synthesis conditions have a remarkable effect on crystalline phases, crystallite size, and surface area; as a result, the photocatalytic activity of TiO_2 is modified as well. López and Gómez [25] report differences in optoelectronic properties between TiO_2 (anatase phase) and commercial TiO_2 Degussa P25 (80%wt anatase and 20%wt rutile phases). The band gap energy value depends on the measurement method, model to fit data and electronic transition type. TiO_2 and CeO_2 have indirect and direct electronic transition, respectively [26,27]. We consider a lack of information with respect to the electronic transition type for TiO_2-CeO_2 semiconductor heterojunction.

TiO_2 and CeO_2 nanoparticles display similar zeta potential behavior with pH, point of zero charge (PZC) for TiO_2 are between 6–8.2 mV [28] and for CeO_2 around 6–8.6 mV [29,30], thus zeta potential analysis won´t provide enough information regarding the location of the CeO_2 and TiO_2. Sol-gel synthesis produces TiO_2 and CeO_2 with different crystalline phases. On one side, Mohammadi et al. [31] studied physical, chemical and electrical characteristics of nanostructured TiO_2-CeO_2 thin films and powders. Ce:Ti molar ratio was related to phase composition and crystallite size; moreover, the study confirmed the formation of titanium and cerium mixed oxides. On the other side, some authors claim that Ce acts effectively as a doping agent in TiO_2 and forms interband states, which improves the photocatalytic activity [31]. Nevertheless, Ce and Ti atoms have large size differences and TiO_2 lattice cannot accommodate Ce atoms. Ti coordination number is 6 in TiO_2 anatase tetragonal structure, and 8 for Ce in CeO_2 fluorite cubic structure. Ce^{4+} and Ti^{4+} ionic sizes are 0.093 nm and 0.068 nm, respectively. According this numbers, Ce lattice substitution in TiO_2 crystal lattice is highly unlikely [9,14,15]. Both studies show enhanced yield in photocatalytic activity, but they offer opposite hypotheses: the first one affirms the formation of Ti-Ce mixed oxides and the last one, asserts that Ce atoms can be into the TiO_2 lattice as doping. In those cases, it is difficult to understand the effect of the crystalline structure in the optoelectronic properties.

In order to enhance photocatalytic activity of TiO_2, we synthesize TiO_2-CeO_2 nanoparticles and study their morphology, crystalline phases and optoelectronic properties. With the aim of measuring the photocatalytic activity, we used methylene blue as an organic pollutant, and comparisons between synthesized TiO_2-CeO_2 semiconductors with commercial TiO_2 (Degussa P25) are also presented to test the efficiency of our nanoparticles. TiO_2-CeO_2 nanoparticles demonstrate their potential as a suitable photocatalytic material to use under the sunlight.

2. Materials and methods

2.1. Materials

Titanium tetraisopropoxide (TTIP) with 97% purity from Sigma Aldrich® and cerium nitrate hexahydrate ($CeNO_3$) with 99.5% purity from REacton Alfa Aesar® were used as TiO_2 and CeO_2 precursors, respectively. TTIP chemical stabilization was performed by complexation reactions with acetylacetone (Acac) from Merck®. Isopropanol (IsoOH) from Merck® was used as a solvent. The CeO_2 nanoparticles dispersion was achieved using polyethylene glycol (PEG) with 1500 Mw from Alfa Aesar®. Water pH was modified with glacial acetic acid and sodium hydroxide, both from Merck®. Commercial TiO_2 nanoparticles Degussa P25 from Sigma Aldrich® was used for comparative aims. Methylene blue was supply by Panreac®.

2.2. Sol-gel Synthesis of TiO_2 and TiO_2-CeO_2 nanoparticles

For Acac:TTIP solution was used 2:1 M ratio and 1:4 for IsoOH:TTIP. TTIP was added to this solution under stirring, until a homogeneous solution was obtained. The resulting solution was loaded into a syringe to add drop-wise in pH 2 acidulated water under vigorous stirring for 2 h. Water:TTIP molar ratio was 20:1 for all the experiments. For TiO_2-CeO_2 nanoparticles, CeO_2 precursor was dissolved in acidulated water from 0.1, 0.25, 0.5, 1, 3 and 5 mol%. After gel formation, a rotary evaporator Heidolph Hei-VAP Precision® at 60 °C and 70 rpm was used to concentrate the samples. Those powders were washed with distilled water and ethanol, and then dried at 80 °C for 12 h. Calcination was realized in oxidant atmosphere with 5 °C/min^{-1} heating rate until 400 °C for 2 h.

2.3. Synthesis of CeO_2 nanoparticles

The precipitation method was carried out for the synthesis of CeO_2. Initially, 0.01 M $CeNO_3$ and 0.1 M NaOH solutions were prepared. Different amounts of PEG (1%, 3% and 5% v/v) were dissolved in NaOH solution. Then, the $CeNO_3$ solution was charged into a syringe and added drop-wise into the alkali solution. The final solution was stirred for 2 h at room temperature and the metallic hydroxide was separated by centrifugation and thereafter dried at 80 °C. Finally, calcination was carried out at 400 °C for 2 h at heating rate of 5 °C/min.

2.4. Characterization of nanoparticles

Chemical modification of TiO_2 precursor by Acac was analyzed by Fourier transform infrared spectroscopy (FTIR) from 4000 to 400 cm^{-1}, in a Perkin Elmer Spectrum Two model.

Crystalline phases, interplanar distance and crystallite size of nanoparticles were studied by X-ray diffraction in 2θ = 20–80°. XRD patterns were obtained with an X'pert PANanalytical Empyrean series II X-ray diffractometer with Cu Kα1 (λ = 1,540598 Å) and Kα2 (λ = 1,544426 Å).

The morphology and particle size of nanoparticle samples were analyzed by Transmission electron microscopy (TEM, FEI Tecnai G2 F20). TEM samples were prepared adding three drops of acetone with dispersed nanoparticles in Lacey/carbon copper grids 200 mesh (Electron Microscopy Sciences). ImageJ software 1.46r version was used to measure the particle diameter (n = 50) in 3 images of each sample.

BET surface area was measured in NOVA 2200e Quantachrome Instruments sortometer. 100 mg of each sample were degasificated for 13 h at 200 °C and nitrogen adsorption-desorption isotherm was analyzed through BET method in the range of 0.05–0.3 relative pressures.

The optoelectronic properties of nanoparticles were determined by diffuse reflectance spectroscopy (Varian Cary 300 UV–Vis). The spectra of the powder samples were obtained with barium sulphate pellets with 5% w/w of TiO_2-CeO_2 nanoparticles.

2.5. Photocatalytic degradation of methylene blue

TiO_2-CeO_2 photocatalytic activity was compared with commercial TiO_2 Degussa (P25) by means of methylene blue (MB) degradation. Generally, P25 is used as a standard substance for photocatalytic degradation. 100 mL of 400 ppm MB solution were added to a beaker with 100 mg of TiO_2-CeO_2 nanoparticles. This process was repeated for the whole composition range of the nanoparticles: Commercial TiO_2, TiO_2-CeO_2, 0, 0.1, 0.25, 0.5, 1, 3, 5% mole and CeO_2 nanoparticles.

During the first 30 min, the MB solution with nanoparticles was put in darkness to promote the adsorption equilibrium of pollutant molecules on the particle surface. Then, the solutions were placed in a chamber with xenon lamps to simulate the solar radiation (Q-LAB Q SUN Xenon test chamber Model Xe-1). Every 30 min, aliquots (~ 5 mL) were taken to obtain the absorption spectrum, which is related to MB concentration by means of calibration curve previously made. An Advantec filter with a 0.20 μm pore size was used to separate the particles. The degradation efficiency was calculated by the equation reported by Ameen et al. [5].

$$Degradation(\%) = \left(\frac{C_0 - C}{C_0}\right)*100 = \left(\frac{A_0 - A}{A_0}\right)*100 \quad (1)$$

Where C_0 is the initial concentration, C is the concentration at a specific time, A_0 is the initial absorbance and A is the absorbance at a specific time.

3. Results and discussion

3.1. Chemical modification of TiO_2 precursor

Due to the reactivity with humidity of metal alkoxides, it was necessary to form stable precursor molecules from complexations reactions. TiO_2-CeO_2 stable gels without precipitated particles were obtained by sol-gel method with Acac as TTIP stabilizing agent.

The infrared spectrum of TiO_2 gel (Fig. 1a) shows bands related to methyl groups, which are present in isopropoxy and acetylacetonato groups [34,35]. Bands around 1017 and 615 cm^{-1} are associated to C-O stretching vibrations of isopropoxy group bound to titanium and Ti-isopropoxide bonds, respectively. Thus, some isopropoxy groups remain bound to titanium [19]. The band in 1714 cm^{-1} corresponds to C-O vibration of free Acac. Therefore, Acac was not consumed totally in the complexation reaction. Around 1590 and 1530 cm^{-1}, there are bands related to C–O and C–C bonds of acetylacetonato group bound to titanium. Ti–O bonds of Ti–O (Acac) groups appear in 488 and 430 cm^{-1}, due to the chemical modification of TTIP to form new precursor molecules, as reported by Brinker and Scherer [17].

TiO_2-CeO_2 gel samples do not show changes in bands related to functional groups (Fig. 1b). Besides, there is no evidence of bands associated to CeO_2 precursor due to its low content.

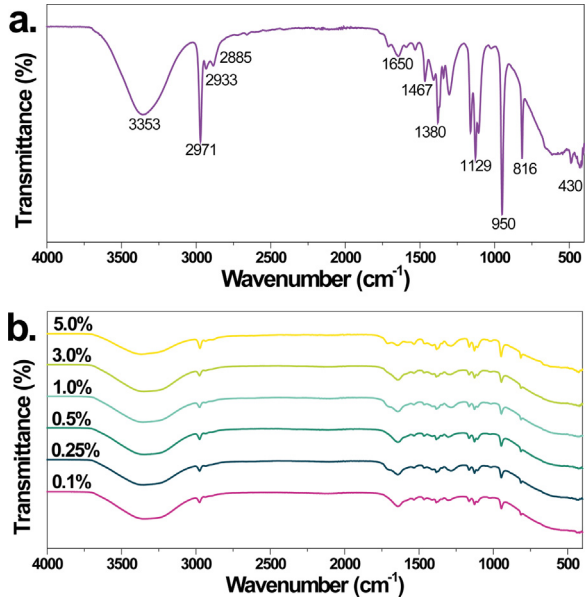

Fig. 1. FTIR spectra of a) TiO_2-Acac modified gel and b) TiO_2-CeO_2 gels in the evaluated composition range.

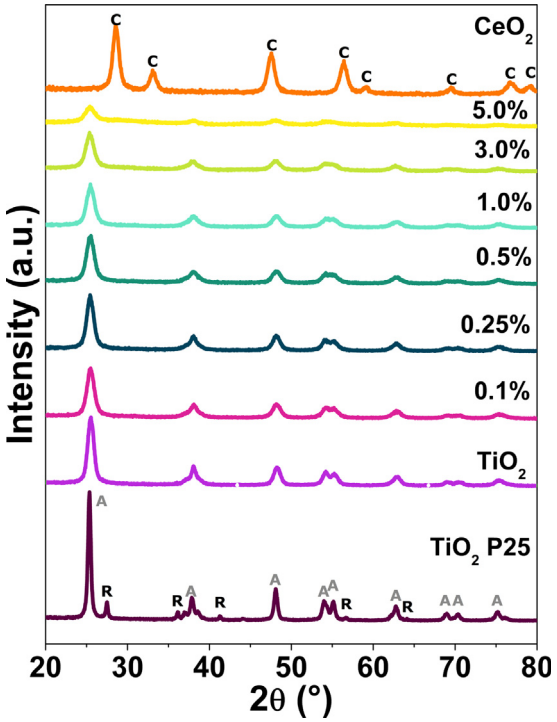

Fig. 2. XRD patterns of commercial TiO_2, TiO_2-CeO_2 nanoparticles in different proportions, and CeO_2 (3% PEG) nanoparticles. Crystalline phases A: anatase TiO_2, R: rutile TiO_2 and C: cubic CeO_2.

3.2. Crystalline properties

Fig. 2 shows the XRD patterns of TiO_2-CeO_2 nanoparticles with different CeO_2 content compared to commercial TiO_2 and CeO_2 nanoparticles. Commercial TiO_2 XRD patterns reveal anatase and rutile phases proportion 85/15, estimated by means of the Spurr equation [36]. CeO_2 nanoparticles with 0%, 1%, 3%, and 5% PEG evidence typical crystalline fluorite phase. CeO_2 nanoparticles synthesized with addition of 3% PEG was chosen to compare with TiO_2-CeO_2 nanoparticles due to its high dispersion and crystalline characteristics.

TiO_2 and TiO_2-CeO_2 nanoparticles present anatase phase, although in high CeO_2 contents, it is possible to observe a small shoulder ($2\theta = 28^\circ$) associated to fluorite or cubic phase formation in TiO_2-CeO_2 nanoparticles. Other authors have reported no-evidence of CeO_2 diffraction peaks [11,37], which is related to ceria low quantities in TiO_2-CeO_2 samples or too small CeO_2 particle size to be detected by XRD [37]. We attempted with Raman to detect CeO_2 in TiO_2 system, but under 5 mol% CeO_2 there is no evidence of fluorite phase.

The anatase main diffraction peak ($2\theta = 26^\circ$) in TiO_2-CeO_2 samples (Fig. 2) shows a decrease in peak intensity with CeO_2 content, which is related to crystallite size decrease when CeO_2 content increases. Similar results were observed by Ghasemi et al. [12]. The reduction in crystallite size by CeO_2 content is due to CeO_2 sol-gel synthesis, which avoids the particles coagulation and retards the crystallite growth during the thermal treatment [12,39].

The interplanar spacing, cell parameters and crystallite size of TiO_2-CeO_2 samples are summarized in Table 1. If a dopant ion is introduced susbtitutionally or interstitially, it is expected a large lattice deformation [13–15]. In our case, ionic radius of Ce^{4+} (0.092 nm) is larger than that of Ti^{4+} (0.064 nm) but smaller than oxygen (0.132 nm), in this case cerium ions can be introduced substitutionally into the matrix, producing some deformation of the lattice structure. Cell parameters for as-prepared materials (Table 1), show minimal variations; as a consequence, there is no alteration or deformation in TiO_2 crystal lattice by the inclusion of Ce atoms, as other authors have reported [32,40], thus

Table 1
Crystalline characteristics of TiO_2-CeO_2 nanoparticles.

Sample	Interplanar spacing (nm)		Cell parameters (nm)		Crystallite size (Å)
	d_{001}	d_{200}	a	c	
TiO_2 P25	3.51	1.89	3.78	9.47	275
TiO_2	3.49	1.89	3.77	9.20	120
TiO_2-CeO_2 0.1%	3.49	1.89	3.76	9.21	103
TiO_2-CeO_2 0.25%	3.50	1.89	3.78	9.29	103
TiO_2-CeO_2 0.5%	3.50	1.89	3.78	9.26	94
TiO_2-CeO_2 1.0%	3.50	1.89	3.78	9.22	90
TiO_2-CeO_2 3.0%	3.50	1.89	3.78	9.32	88
TiO_2-CeO_2 5.0%	3.50	1.89	3.79	9.20	65
CeO_2[a]	3.12	5.41	122		

[a] CeO_2 Interplanar spacing was calculated for (011) crystallographic plane.

in our case substitutional solubility of Ce in Ti-O lattice is not possible. In the case of ions introduced susbtitutionally in the network, oxygen deficiency (OD) are produced, as it was reported by Rodriguez-Talavera [15], but this OD promotes the transition from anatase to rutile. In XRD results only anatase phase is observed. In the case of ceria, only fluorite structure is detected, in spite of the change from Ce^{4+} to Ce^{3+} creating oxygen vacancies, this change did not affect the crystal structure [16]. Moreover, there is no evidence of mixed oxide

3.3. Morphology of nanoparticles

Fig. 3 shows TEM micrographs of TiO_2, TiO_2-CeO_2 and CeO_2 nanoparticles with electron diffraction patterns. TiO_2 nanoparticles with a crystalline spacing length of 0.368 ± 0.007 nm corresponding to plane (1 0 1) (Fig. 3a) do not show a defined geometric shape, but present a heterogeneous surface and its electron diffraction pattern corresponds to TiO_2 anatase phase (Fig. 3b) as it was also observed in XRD results (Fig. 2). These morphological features were encountered for all the TiO_2-CeO_2 nanoparticles in the evaluated composition range (0.1–5% mole CeO_2). In Fig. 3c, it is disclose TiO_2-CeO_2 0.25% images, as an example, with interplanar distances 0.371 ± 0.003 nm corresponding to plane (1 0 1). Otherwise CeO_2 sample (Fig. 3e) interplanar distances 0.332 ± 0.005 nm corresponding to plane (1 1 1). display rounded nanoparticles with less surface heterogeneities and the Fig. 3f exhibits the electron diffraction associated to CeO_2 fluorite or cubic phase. It is remarkable to note that in Fig. 3d, electron diffraction pattern of TiO_2-CeO_2 0.25% sample is mainly associated to TiO_2 anatase phase, also, diffraction spots can be appreciated near the high intensity electron diffraction pattern A(1 0 1) related to CeO_2 cubic fluorite phase in C(1 1 1) and C(2 0 0) crystallographic planes. This feature was not observed in XRD patterns for TiO_2-CeO_2 nanoparticles due to low CeO_2 content or small particle size in samples.

Nanoparticles BET isotherms are showed in Fig. 4. The large plateau in the isotherms until relative pressure 0.8 is achieved can be explained by low multilayer adsorption [41]. From that value on, the volume adsorbed increases quickly by the response of mesoporous filling (2–50 nm pore size). The presence of mesoporous is confirmed by the type H1 hysteresis and associated with a narrow distribution of uniform pores [42]. According to Raj et al. [43] and IUPAC [44], commercial TiO_2 exhibits a type *IIb* isotherm with hysteresis loop, typical of low porous or macroporous samples (pore size higher than 50 nm). CeO_2 presents a similar behavior in type *IIb* isotherm and macroporous samples.

Sol-gel synthetized TiO_2 and TiO_2-CeO_2 present type *IVa* isotherms with H1 hysteresis loop typical of mesoporous materials (Fig. 4) [45]. At very low relative pressure, sol-gel TiO_2 and TiO_2-CeO_2 nanoparticles adsorb a large volume of nitrogen in comparison to commercial TiO_2 adsorption. As a result, the differences are associated with larger size microporous or wider pore size distribution than the characteristic of commercial TiO_2. At high relative pressures, there is a slow increase in adsorbed volume related to wide mesoporous size distribution in TiO_2 and TiO_2-CeO_2 samples. Moreover, hysteresis observed in these samples are wider because of the complex structures with different size and shape pores that characterize surface heterogeneity [42].

These results are consistent with the morphological attributes observed in TEM images (Fig. 3). Since pollutant degradation depends on the adsorption of molecules over nanoparticles surface, a high surface area will increase the quantity of available adsorbed molecules to be degraded. Thus, the heterogeneous surface related to a high surface area in TiO_2-CeO_2 synthesized nanoparticles is an advantage to improve the photocatalytic activity.

In Fig. 5, a high BET surface area is associated to TiO_2 and TiO_2-CeO_2 nanoparticles samples with low particle size and irregular or rough particle surface. Additionally, low BET surface area for commercial TiO_2 is 76.55 $m^2\ g^{-1}$ and for CeO_2 nanoparticles is 38.09 $m^2\ g^{-1}$, with a low mesoporosity and a strong macropores response.

Despite expecting a high surface area of commercial TiO_2 due to its main application in photocatalytic degradation of pollutants, this feature was not observed. We obtained smaller TiO_2-CeO_2 particle sizes than the values already reported [8,37], because the sol-gel method using titanium complex precursor modified with Acac generates stable gels which produce smaller nanoparticles. Moreover, TiO_2-CeO_2 synthesized nanoparticles have twice the surface area (157 $m^2\ g^{-1}$) than the commercial TiO_2. From that, TiO_2-CeO_2 nanoparticles with high surface area could exhibit superior performance for photocatalytic applications.

CeO_2 exhibits lower BET surface area in spite of small particle size, due to smooth surface as it was observed in TEM images (Fig. 3) and macroporosity characteristics (Fig. 4).

3.4. Optoelectronic properties

Powders diffuse reflectance spectra for TiO_2-CeO_2 samples are showed in Fig. 6a. TiO_2 sol-gel and commercial TiO_2 present similar behaviors due to the effect of radiation. Both samples exhibit a change in reflectance spectrum slope around 400 nm. Starting from this value and reading towards lower wavelengths, reflectance decreases and TiO_2 samples begin to absorb UV radiation, precisely where TiO_2 displays its photocatalytic activity. Likewise, CeO_2 shows a reduction in reflectance at 700 nm involving a high activity in the visible range. CeO_2 performs a synergic effect on TiO_2 optoelectronic properties which depend on CeO_2 content [9]. TiO_2-CeO_2 0.1% slope is slowly affected around 400 nm; when CeO_2 content increases to 0.25% mole, the slope changes at higher wavelengths. For nanoparticles with high CeO_2 content as 5%, a greater absorption shifts at visible radiation and a similar optoelectronic behavior to CeO_2 was observed. Band gap energy were calculated using the Kubelka-Munk function and Tauc plots [51] (Fig. 6b).

Anatase TiO_2 presents a band gap indirect transition, but fluorite CeO_2 displays a direct transition. In literature reviewed, some authors took direct or indirect transition interchangeably [38,39,46,48,52]. However, there is a marked difference between band gap values depending on electronic transition considered (Fig. 7). For indirect transition, commercial TiO_2 and TiO_2 sol-gel band gap values are 3.24 eV and 3.21 eV, respectively, similar as values reported 3.26 eV [22,25].

CeO_2 content in TiO_2-CeO_2 decreases the band gap energy until the values get close to CeO_2 band gap. Even samples with minimal CeO_2 content (0.1%) show lower band gaps than TiO_2, but TiO_2-CeO_2 5% has a similar band gap energy to CeO_2. These results are related to reflectance spectra (Fig. 6), because there is a red shift at high wavelengths due to the presence of CeO_2 in TiO_2-CeO_2 nanoparticles that

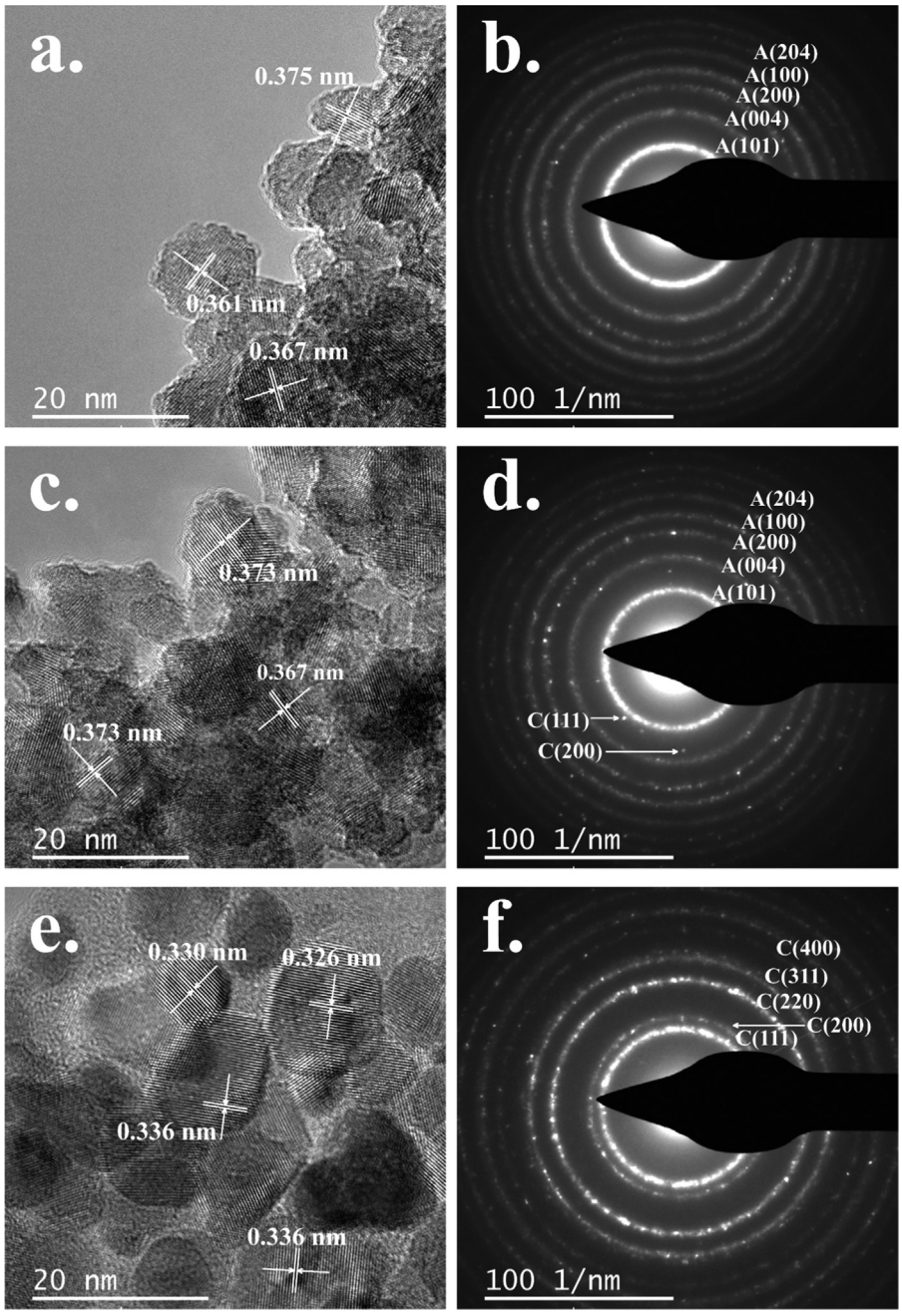

Fig. 3. TEM micrographs of TiO_2-CeO_2 and CeO_2 nanoparticles. a) TiO_2 nanoparticles with interplanar distance of 0.376 nm for the anatase phase A (1 0 1), b) SAED pattern with indexed planes of TiO_2 in anatase phase (A), c) TiO_2-CeO_2 0.25% nanoparticles, the interplanar distances of TiO_2 in anatase phase are between 0.363 and 0.373 nm, d) SAED pattern with indexed planes of TiO2 in anatase phase (A) and CeO_2 in cubic fluorite phase (C), e) CeO_2 nanoparticles with interplanar distance of 0.33 nm in cubic fluorite phase with crystal pattern at C(1 1 1), and f) SAED pattern with indexed planes of CeO_2 in cubic phase (C). All the interplanar distances were measure by mean of image analysis using Gatan Microscopy Suite Software.

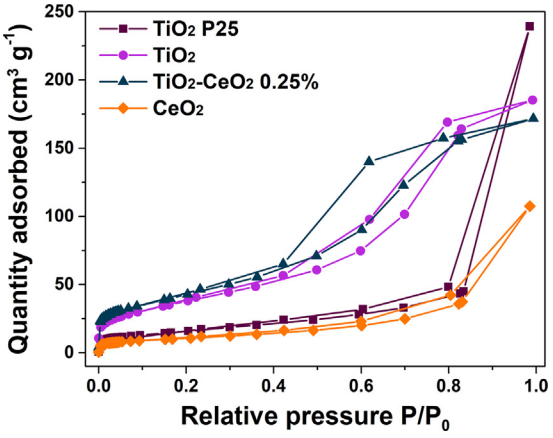

Fig. 4. Nitrogen adsorption-desorption isotherms of TiO_2-CeO_2 powders.

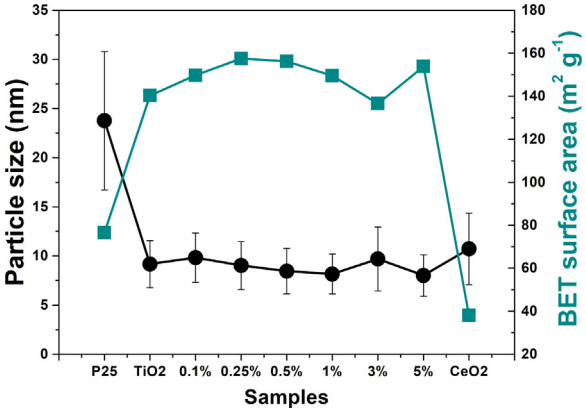

Fig. 5. Particle size and BET surface area of commercial TiO_2, TiO_2-CeO_2 and CeO_2 nanoparticles.

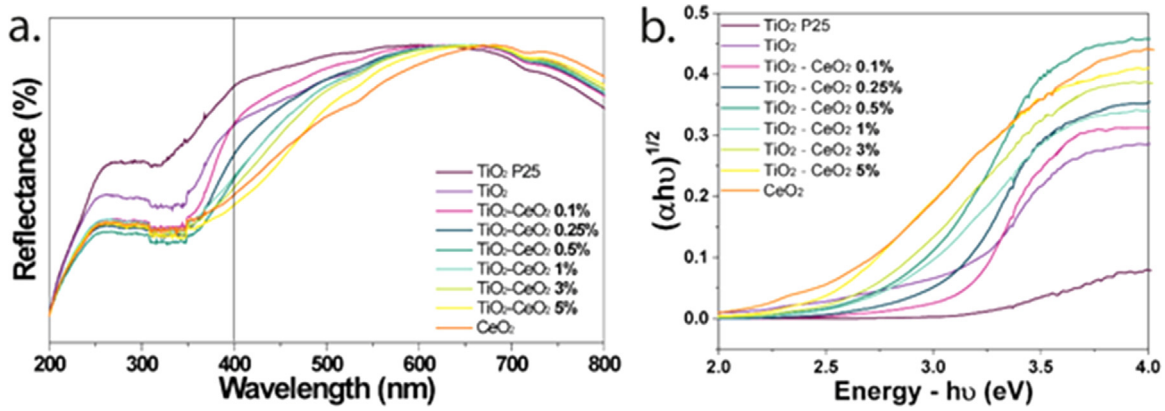

Fig. 6. a. Diffuse reflectance spectra of TiO_2-CeO_2 nanoparticles and b. Tauc plot derived from the Kubelka-Munk function for TiO2-CeO2 nanoparticles using DR-Uv–vis spectrum.

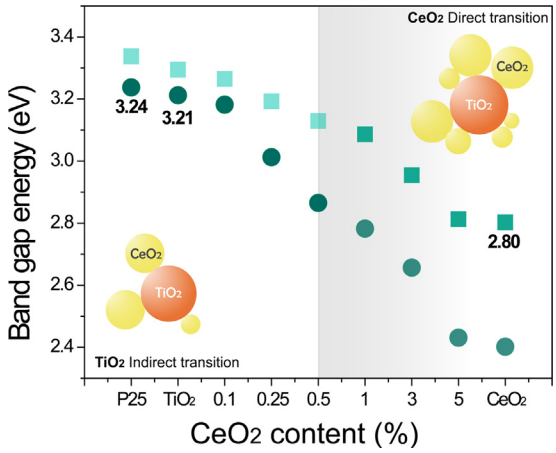

Fig. 7. Band gap energy of TiO_2-CeO_2 nanoparticles assuming the direct and indirect electronic transitions.

implies a narrow band gap. These behave indicates a semiconductors heterojunction and a potential application under visible radiation [7].

Tauc plots only exhibit one slope related to the response of TiO_2 and CeO_2. Moreover, the evaluated semiconductors behave as a solid solution of TiO_2-CeO_2 in synthesized compositions until CeO_2 5% mole. Above this CeO_2 content, Contreras-García et al. [48] found that for TiO_2-CeO_2 samples with CeO_2 content 5%, 10% and 15% mole, anatase and fluorite phases act individually as independent contributors with two slopes in Tauc plots, losing their synergic effect in TiO_2-CeO_2 optoelectronic response.

There are two possible ways to explain this enhanced photocatalytic response in visible light. One alternative is by Ce replacement: this happens when the Ce atom replaces a Ti atom in TiO_2 crystal lattice, achieving mixed oxides, as other authors have reported [28,37,53]. That lattice modification creates states between the valence and the conduction energy bands of TiO_2. Ce and Ti mixed oxides can be confirmed by XDR; in the case of Ce doped TiO_2, an increase in interplanar distance of TiO_2 should be expected. According to our results, there is no evidence of mixed oxides. Only anatase and fluorite phases were confirmed by XRD analysis. Besides, the interplanar distance (*d*) and cell parameters evaluated (*a, b* and *c*) do not present significant changes (Table 1). Ce lattice substitution in TiO_2 crystal lattice is highly unlikely because Ti coordination number is 6 in TiO_2 anatase tetragonal structure, 8 for Ce in CeO_2 fluorite cubic structure and Ti and Ce ionic sizes are 0.093 nm and 0.068 nm for Ce^{4+} and Ti^{4+} ion, respectively [9].

The second alternative is based on TiO_2-CeO_2 semiconductor coupling. In some reports, it is considered as the main explanation to this behavior because TiO_2-CeO_2 band gap values reveal a single intermediate response between individual values of metal oxides [5,9,48]. Due to CeO_2 nanoparticles are on TiO_2 surface, the optimal covering on TiO_2 surface to achieve high efficiencies in photocatalytic applications depends on CeO_2 content. On this basis, a higher CeO_2 content restricts the optoelectronic properties of modified TiO_2 and CeO_2 response prevail over TiO_2 (Fig. 8). In our systems, when CeO_2 optoelectronic properties dominate over TiO_2 is in the range between 1% up to 5% mole. In this composition range, it is necessary to consider direct band

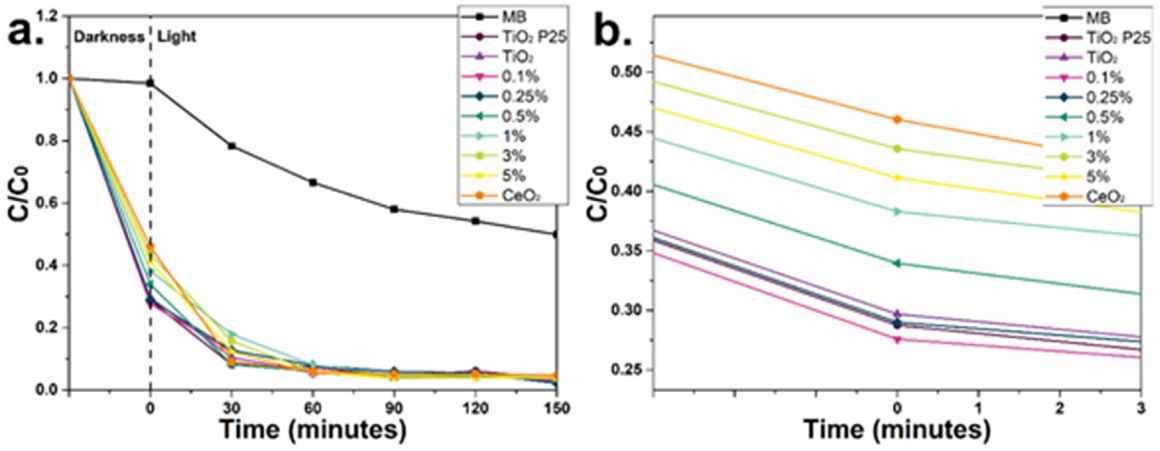

Fig. 8. a) Degradation of methylene blue solution by visible light for TiO_2-CeO_2 nanoparticles and b) Detail of the MB concentration after the darkness stage (related to MB adsorption).

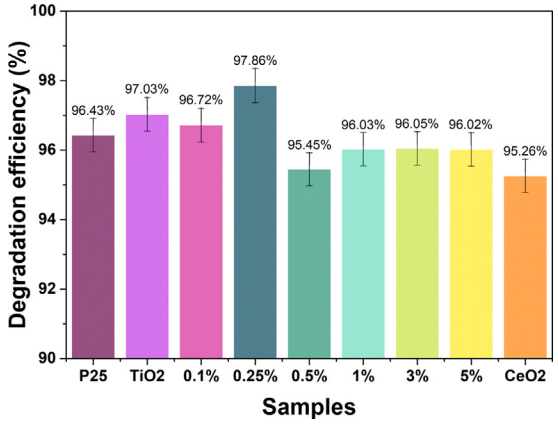

Fig. 9. Degradation efficiency of methylene blue after 150 min under visible light.

gap type to describe the optoelectronic behavior. In comparison with compositions lower than 1%, in which TiO_2 nanoparticles are not completely cover for CeO_2, an indirect transition need to be used to fit data. Effective TiO_2-CeO_2 band gap need to be estimated by experimental procedures, due to changes in the optoelectronic response produced by the surface coating. Those results suggest that TiO_2 and CeO_2 exhibit a semiconductor heterojunction with enhanced optoelectronic properties under visible light.

3.5. TiO_2-CeO_2 photocatalytic activity by simulated sunlight

TiO_2-CeO_2 degradation studies in visible light during 150 min of simulated solar radiation are shown in Fig. 8a. MB concentration decreases by the photocatalytic activity of TiO_2-CeO_2. MB control solution degradation, without catalysts, due to the radiation is about 50%. Despite that MB has been commonly used to determine the photocatalytic activity of different materials [54-57] there are experimental drawbacks associated to MB sensitivity to light that have not been reported so far.

In order to establish adsorption-desorption equilibrium of pollutant on the photocatalyst surface, the MB solution with nanoparticles was put into darkness for 30 min prior to solar radiation. Adsorption is related to the initial concentration (C_0, 0 min radiation) that is detailed in Fig. 8b. Commercial TiO_2 and TiO_2 sol-gel show low concentration of MB solution in the darkness stage, which is associated to a high MB adsorption on nanoparticles surface. On the contrary, CeO_2 nanoparticles exhibit lower adsorption capacity than TiO_2. Thus, MB adsorption on TiO_2-CeO_2 nanoparticles surface depends on CeO_2 content. According to Wandre et al. [22], the greater the adsorption capacity of molecules on nanoparticles surface, the higher the pollutant degradation that will take place, therefore increasing the photocatalytic activity. TiO_2-CeO_2 nanoparticles with low CeO_2 content (0.1% up to 0.5% mole) show high MB adsorption capacity, like TiO_2, while a low adsorption capacity was noticed at high CeO_2 content. Those results are correlated to BET surface area (Fig. 5) and band gap values (Fig. 8).

MB degradation efficiency is showed in Fig. 9. Generally, efficiency values around 95% were found for all samples in the evaluated composition range. CeO_2 has the lowest MB degradation compared to other samples, due to poor MB adsorption capacity. Commercial TiO_2, used in photocatalytic applications, presented a slightly lower efficiency than sol-gel synthesized TiO_2, as a result of differences in BET surface areas for both samples. A higher surface area of sol-gel TiO_2 related to high mesoporosity and greater adsorption capacity implies favorable photocatalytic responses. TiO_2-CeO_2 shows values between TiO_2 and CeO_2 efficiencies. However, TiO_2-CeO_2 0.25% nanoparticles display better efficiency (97.86%) than commercial TiO_2, this characteristic is attributed to its band gap value (3.01 eV-indirect transition), high MB adsorption capacity and high surface area (157.54 m^2 g^{-1}) that promotes its photocatalytic activity in solar light MB degradation. This optimal composition is attributed to the reduction in the e^-/h^+ pairs recombination when 0.25% CeO_2 is incorporated on TiO_2. Magesh et al. [9] found that in a thin layer of CeO_2 on TiO_2 surface the excited electrons created in CeO_2 due to visible light irradiation can be transfer immediately to TiO_2.

4. Conclusions

CeO_2 modified TiO_2 nanoparticles were synthesized by sol-gel method. Stable gels of TiO_2-CeO_2 were achieved through the formation of stable precursor molecules. These molecules were obtained by complexation reaction of TTIP with Acac, which was promoted in acid medium by the addition of glacial acetic acid. TiO_2-CeO_2 nanoparticles have anatase and fluorite crystalline phases. CeO_2 in TiO_2-CeO_2 nanoparticles has a strong influence on the crystallinity. As CeO_2 content increases, the growth of TiO_2 crystallite is restricted.

Average particle size of TiO_2-CeO_2 nanoparticles is 10 nm, smaller than commercial TiO_2 nanoparticles. Heterogeneous surface, small particle size and mesoporosity lead to high BET surface area of TiO_2 and TiO_2-CeO_2 nanoparticles, compared to commercial TiO_2 and CeO_2 nanoparticles.

Nanoparticles exhibited a shift in the absorption range of UV radiation towards visible light range, which is related to band gap energy of TiO_2-CeO_2 nanoparticles depending upon CeO_2 content. TiO_2-CeO_2 band gap decreases when CeO_2 content increases. However, CeO_2 optoelectronic properties predominate in samples with high CeO_2 content. TiO_2 and CeO_2 ionic size and coordination number make the mixed oxides formation or doping TiO_2 by Ce unlikely. Semiconductors heterojunction is achieved for TiO_2-CeO_2 nanoparticles, which enhances optoelectronic properties in visible light.

MB solution evaluated as polluting organic model substance, had an average degradation of 95% in presence of TiO_2-CeO_2 nanoparticles that were activated by simulated solar radiation. TiO_2-CeO_2 photocatalytic activity depends on the optoelectronic properties and MB adsorption capacity. TiO_2-CeO_2 adsorption capacity increases and leads to a high photocatalytic activity. Our results display that the system TiO_2-CeO_2 0.25% had better photocatalytic performance than commercial TiO_2.

Acknowledgements

Authors would like to thank Universidad EAFIT for the financial support in this project.

References

[1] J.L. Vivero-Escoto, Y.-D. Chiang, K.C.W. Wu, Y. Yamauchi, Recent progress in mesoporous titania materials: adjusting morphology for innovative applications, Sci. Technol. Adv. Mater. 13 (2012) 13003.
[2] Y. Lan, Y. Lu, Z. Ren, Mini review on photocatalysis of titanium dioxide nanoparticles and their solar applications, Nano Energy 2 (2013) 1031–1045.
[3] A.L. Linsebigler, G. Lu, J.T. Yates Jr, Photocatalysis on TiO_2 surfaces: principles, mechanisms, and selected results, Chem. Rev. 95 (1995) 735–758.
[4] Y. Bessekhouad, D. Robert, J.V. Weber, Bi_2S_3/TiO_2 and CdS/TiO_2 heterojunctions as an available configuration for photocatalytic degradation of organic pollutant, J. Photochem. Photobiol. A Chem. 163 (2004) 569–580.
[5] S. Ameen, M.S. Akhtar, H.-K. Seo, H.-S. Shin, Solution-processed CeO_2/TiO_2 nanocomposite as potent visible light photocatalyst for the degradation of bromophenol dye, Chem. Eng. J. 247 (2014) 193–198.
[6] M.R. Mohammadi, D.J. Fray, Synthesis and characterisation of nanosized TiO_2–ZrO_2 binary system prepared by an aqueous sol–gel process: physical and sensing properties, Sens. Actuators B Chem. 155 (2011) 568–576.
[7] H. Wang, L. Zhang, Z. Chen, J. Hu, S. Li, Z. Wang, J. Liu, X. Wang, Semiconductor heterojunction photocatalysts: design, construction, and photocatalytic performances, Chem. Soc. Rev. 43 (2014) 5234–5244.
[8] A. Trovarelli, Catalytic properties of ceria and CeO_2-containing materials, Catal. Rev. 38 (1996) 439–520.
[9] G. Magesh, B. Viswanathan, R.P. Viswanath, T.K. Varadarajan, Photocatalytic behavior of CeO_2-TiO_2 system for the degradation of methylene blue, Indian J. Chem.

Sect. A Inorganic, Phys. Theor. Anal., vol. 48, n.d., pp. 480–488.
[10] U. Qureshi, C.W. Dunnill, I.P. Parkin, Nanoparticulate cerium dioxide and cerium dioxide–titanium dioxide composite thin films on glass by aerosol assisted chemical vapour deposition, Appl. Surf. Sci. 256 (2009) 852–856.
[11] B. Zhao, B. Shi, X. Zhang, X. Cao, Y. Zhang, Catalytic wet hydrogen peroxide oxidation of H-acid in aqueous solution with TiO_2–CeO_2 and Fe/TiO_2–CeO_2 catalysts, Desalination 268 (2011) 55–59.
[12] S. Ghasemi, S.R. Setayesh, A. Habibi-Yangjeh, M.R. Hormozi-Nezhad, M.R. Gholami, Assembly of CeO_2–TiO_2 nanoparticles prepared in room temperature ionic liquid on graphene nanosheets for photocatalytic degradation of pollutants, J. Hazard. Mater. 199 (2012) 170–178.
[13] M. Hirano, T. Joji, M. Inagaki, Direct formation of iron(III)-doped titanium oxide (anatase) by thermal hydrolysis and its structural property, J. Am. Ceram. Soc. 87 (2004) 35–41.
[14] Q.-Z. Yan, X.-T. Su, Z.-Y. Huang, C.-C. Ge, Sol–gel auto-igniting synthesis and structural property of cerium-doped titanium dioxide nanosized powders, J. Eur. Ceram. Soc. 26 (2006) 915–921.
[15] R. Rodriguez-Talavera, S. Vargas, R. Arroyo, R. Montiel, E. Haro, Modification of the phase transition temperatures in titania doped with various cations, J. Mater. Res. 12 (1997) 439–443.
[16] S. Phokha, S. Hunpratub, N. Chanlek, S. Sonsupap, S. Maensiri, Synthesis, characterization and electrochemical performance of carbon/Ni-doped CeO_2 composites, J. Alloy. Compd. 750 (2018) 788–797.
[17] C.J. Brinker, G.W. Scherer, Sol-Gel Science: The Physics and Chemistry of Sol-Gel Processing, Academic press, San Diego, USA, 2013.
[18] J. Livage, C. Sanchez, Sol-gel chemistry, J. Non Cryst. Solids 145 (1992) 11–19.
[19] A. Leaustic, F. Babonneau, J. Livage, Structural investigation of the hydrolysis-condensation process of titanium alkoxides $Ti(OR)_4$ (OR = OPr-iso, OEt) modified by acetylacetone. 1. Study of the alkoxide modification, Chem. Mater. 1 (1989) 240–247.
[20] A. Leaustic, F. Babonneau, J. Livage, Structural investigation of the hydrolysis-condensation process of titanium alkoxides $Ti(OR)_4$ (OR = OPr-iso, OEt) modified by acetylacetone. 2. From the modified precursor to the colloids, Chem. Mater. 1 (1989) 248–252.
[21] C. Sanchez, J. Livage, M. Henry, F. Babonneau, Chemical modification of alkoxide precursors, J. Non Cryst. Solids 100 (1988) 65–76.
[22] T.M. Wandre, P.N. Gaikwad, A.S. Tapase, K.M. Garadkar, S.A. Vanalakar, P.D. Lokhande, R. Sasikala, P.P. Hankare, Sol–gel synthesized TiO_2–CeO_2 nanocomposite: an efficient photocatalyst for degradation of methyl orange under sunlight, J. Mater. Sci. Mater. Electron. 27 (2016) 825–833.
[23] X.-W. Niu, Y.-M. Sun, S.-N. Ding, C.-C. Chen, B. Song, Preparation and characterization of novel yellow pigments: hollow TiO_2 spheres doped with cerium, J. Mater. Sci. Mater. Electron. 22 (2011) 1865–1874.
[24] B.S. Shirke, P.V. Korake, P.P. Hankare, S.R. Bamane, K.M. Garadkar, Synthesis and characterization of pure anatase TiO_2 nanoparticles, J. Mater. Sci. Mater. Electron. 22 (2011) 821–824.
[25] R. López, R. Gómez, Band-gap energy estimation from diffuse reflectance measurements on sol–gel and commercial TiO_2: a comparative study, J. Sol-Gel Sci. Technol. 61 (2012) 1–7.
[26] Z. Fan, F. Meng, J. Gong, H. Li, Y. Hu, D. Liu, Enhanced photocatalytic activity of hierarchical flower-like CeO_2/TiO_2 heterostructures, Mater. Lett. 175 (2016) 36–39.
[27] J. Malleshappa, H. Nagabhushana, B.D. Prasad, S.C. Sharma, Y.S. Vidya, K.S. Anantharaju, Structural, photoluminescence and thermoluminescence properties of CeO_2 nanoparticles, Opt. J. Light Electron Opt. 127 (2016) 855–861.
[28] F. Loosli, P. Le Coustumer, S. Stoll, Effect of natural organic matter on the disagglomeration of manufactured TiO_2 nanoparticles, Environ. Sci. Nano 1 (2014) 154–160.
[29] X. Song, N. Jiang, Y. Li, D. Xu, G. Qiu, Synthesis of CeO_2-coated SiO_2 nanoparticle and dispersion stability of its suspension, Mat. Chem. Phys. 110 (2008) 128–135.
[30] L. Exbrayat, P. Steyer, C. Rébéré, C. Berziou, C. Savall, P. Ayrault, E. Tertre, G.L. Joly-Pottuz, J. Creus, Electrodeposition of zinc–ceria nanocomposite coatings in alkaline bath, J. Solid State Electrochem. 18 (2014) 223–233.
[31] M.R. Mohammadi, D.J. Fray, Nanostructured TiO_2–CeO_2 mixed oxides by an aqueous sol–gel process: effect of Ce: Ti molar ratio on physical and sensing properties, Sens. Actuators B Chem. 150 (2010) 631–640.
[32] T. Tong, J. Zhang, B. Tian, F. Chen, D. He, M. Anpo, Preparation of Ce–TiO_2 catalysts by controlled hydrolysis of titanium alkoxide based on esterification reaction and study on its photocatalytic activity, J. Colloid Interface Sci. 315 (2007) 382–388.
[34] C.T. Lynch, K.S. Mazdiyasni, J.S. Smith, W.J. Crawford, Infrared spectra of transition metal alkoxides, Anal. Chem. 36 (1964) 2332–2337, https://doi.org/10.1021/ac60218a034.
[35] P.D. Moran, G.A. Bowmaker, R.P. Cooney, K.S. Finnie, J.R. Bartlett, J.L. Woolfrey, Vibrational spectra and molecular association of titanium tetraisopropoxide, Inorg. Chem. 37 (1998) 2741–2748, https://doi.org/10.1021/ic9709436.
[36] R.A. Spurr, H. Myers, Quantitative analysis of anatase-rutile mixtures with an X-ray diffractometer, Anal. Chem. 29 (1957) 760–762.
[37] Z. Liu, B. Guo, L. Hong, H. Jiang, Preparation and characterization of cerium oxide doped TiO_2 nanoparticles, J. Phys. Chem. Solids 66 (2005) 161–167.
[38] H. Abdullah, N.A. Ismail, Z. Yaakob, M.R. Khan, S.A. Rahim, CeO_2-TiO_2 for photoreduction of CO_2 to methanol under visible light: effect of ceria loading, Malays. J. Anal. Sci. 21 (2017) 166–172, https://doi.org/10.17576/mjas-2017-2101-19.
[39] C. Fan, P. Xue, Y. Sun, Preparation of nano-TiO_2 doped with cerium and its photocatalytic activity, J. Rare Earths 24 (2006) 309–313.
[40] S. Watanabe, X. Ma, C. Song, Characterization of structural and surface properties of nanocrystalline TiO_2–CeO_2 mixed oxides by XRD, XPS, TPR, and TPD, J. Phys. Chem. C 113 (2009) 14249–14257.
[41] B.L. Bischoff, M.A. Anderson, Peptization process in the sol-gel preparation of porous anatase (TiO_2), Chem. Mater. 7 (1995) 1772–1778.
[42] J. Rouquerol, F. Rouquerol, P. Llewellyn, G. Maurin, K.S.W. Sing, Adsorption by Powders and Porous Solids: Principles, Methodology and Applications, Academic press, San Diego, USA, 2013.
[43] K.J.A. Raj, B. Viswanathan, Effect of surface area, pore volume and particle size of P25 titania on the phase transformation of anatase to rutile, Indian J. Chem. A 48 (2009) 1378–1382.
[44] K.S.W. Sing, D.H. Everett, R.A.W. Haul, L. Moscou, R.A. Pierotti, J. Rouquerol, T. Siemieniewska, Reporting physisorption data for gas/solid systems, in: Gerhard Ertl, Helmut Knözinger, Ferdi Schüth, Jens Weitkamp (Eds.), Handb. Heterog. Catal. Wiley-VCH Verlag GmbH & Co. KGaA, New Jersey, USA, 2008, , https://doi.org/10.1002/9783527610044.hetcat0065.
[45] K.S.W. Sing, Reporting physisorption data for gas/solid systems with special reference to the determination of surface area and porosity (Recommendations 1984), Pure Appl. Chem. 57 (1985) 603–619.
[46] K.P. Priyanka, S.A. Tresa, O.P. Jaseentha, T. Varghese, Cerium doped nanotitania—extended spectral response for enhanced photocatalysis, Mater. Res. Express 1 (2013) 15003.
[48] M.E. Contreras-García, M.L. García-Benjume, V.I. Macías-Andrés, E. Barajas-Ledesma, A. Medina-Flores, M.I. Espitia-Cabrera, Synergic effect of the TiO_2-CeO_2 nanoconjugate system on the band-gap for visible light photocatalysis, Mater. Sci. Eng. B 183 (2014) 78–85.
[51] S. Wang, J.-H. Yun, B. Luo, T. Butburee, P. Peerakiatkhajohn, S. Thaweesak, M. Xiao, L. Wang, Recent progress on visible light responsive heterojunctions for photocatalytic applications, J. Mater. Sci. Technol. 33 (2017) 1–22.
[52] J. Dhanalakshmi, S. Iyyapushpam, S.T. Nishanthi, M. Malligavathy, D.P. Padiyan, Investigation of oxygen vacancies in Ce coupled TiO_2 nanocomposites by Raman and PL spectra, Adv. Nat. Sci. Nanosci. Nanotechnol. 8 (2017) 15015.
[53] T. Lopez, F. Rojas, R. Alexander-Katz, F. Galindo, A. Balankin, A. Buljan, Porosity, structural and fractal study of sol–gel TiO_2–CeO_2 mixed oxides, J. Solid State Chem. 177 (2004) 1873–1885.
[54] Y.J. Jang, C. Simer, T. Ohm, Comparison of zinc oxide nanoparticles and its nanocrystalline particles on the photocatalytic degradation of methylene blue, Mater. Res. Bull. 41 (2006) 67–77.
[55] Z. Li, W. Shen, W. He, X. Zu, Effect of Fe-doped TiO_2 nanoparticle derived from modified hydrothermal process on the photocatalytic degradation performance on methylene blue, J. Hazard. Mater. 155 (2008) 590–594.
[56] W. Shen, Z. Li, H. Wang, Y. Liu, Q. Guo, Y. Zhang, Photocatalytic degradation for methylene blue using zinc oxide prepared by codeposition and sol–gel methods, J. Hazard. Mater. 152 (2008) 172–175.
[57] M.A. Ahmed, E.E. El-Katori, Z.H. Gharni, Photocatalytic degradation of methylene blue dye using Fe_2O_3/TiO_2 nanoparticles prepared by sol–gel method, J. Alloy. Compd. 553 (2013) 19–29.